Author Accepted Manuscript. This article is published in Phys. Status Solidi B 2019, 256, 1800428,
https://doi.org/10.1002/pssb.201800428

Small-angle neutron scattering and magnetically heterogeneous state in $Sr_2FeMoO_{6-\delta}$

Nikolay Kalanda, Vasil Garamus, Mikhail Zheludkevich, Marta Yarmolich, Maria Serdechnova, Dietmar Christian Florian Wieland, Alexander Petrov, Aliaksandr Zhaludkevich, Nikolai A. Sobolev*

Dr. N. Kalanda, Dr. M. Yarmolich, Dr. A. Petrov, A. Zhaludkevich
Scientific-Practical Materials Research Centre of the NAS of Belarus, P. Brovka str. 19, 220072 Minsk, Belarus
*E–mail: kalanda@physics.by

Dr. V.M. Garamus, Prof. M. Zheludkevich, Dr. M. Serdechnova, Dr. D.C.F. Wieland
Helmholtz–Zentrum Geesthacht: Zentrum für Material- und Küstenforschung GmbH, Max–Planck–Str. 1, D–21502 Geesthacht, Germany

Prof. N.A. Sobolev
Departamento de Física and I3N, Universidade de Aveiro, 3810–193 Aveiro, Portugal,
National University of Science and Technology MISiS, 119049 Moscow, Russia

Keywords: strontium ferromolybdate, superstructure ordering, oxygen non-stoichiometry, magnetization, small-angle neutron scattering

Single-phase strontium ferromolybdate ($Sr_2FeMoO_{6-\delta}$) samples with different degrees of the superstructural ordering of the Fe/Mo cations were obtained from partially reduced $SrFeO_{3-x}$, $SrMoO_4$ precursors by the solid-state technology. The study of the temperature dependences of the magnetization measured in the field-cooling and zero-field-cooling regimes indicated an inhomogeneous magnetic state of the samples. The presence of magnetic regions of different nature has also been revealed by the small-angle neutron scattering. For the $Sr_2FeMoO_{6-\delta}$ samples with different superstructural ordering of the Fe/Mo cations and for all values of the magnetic field induction in the range up to 1.5 T and of the scattering vector in the interval $0.1 > q > 0.005$ Å^{-1}, the analytical dependence $I \sim q^{-\alpha}$ obeys the Porod law ($\alpha \approx 4$), which corresponds to an object with a smooth and well-marked surface and polydisperse grain size. Deviations from the Porod law in the $q > 0.1$ Å^{-1} region and a weakening of the neutron scattering in applied magnetic fields may be ascribed to magnetic inhomogeneities with diameters $D < 6$ nm, which are partially destroyed /oriented by magnetic fields $B \geq 1.5$ T.

1. Introduction

There are numerous potential applications of the $Sr_2FeMoO_{6-\delta}$ double perovskite (SFMO), such as energy-independent magnetic random-access memory (MRAM), magnetic read heads for hard-disk drives, sensitive magnetic-field sensors, electrodes for solid fuel elements [1–3], and others. For these applications, structurally perfect SFMO samples with high values of the Curie temperature, saturation magnetization (M_s), spin polarization degree of conduction electrons (P_s) are needed [4–7]. Thus, the improvement of the technology for obtaining structurally perfect SFMO with reproducible magnetic and electrical properties remains an important problem.

One of the conditions for the existence of a high degree of spin polarization of conduction electrons in SFMO is the presence of superstructural ordering of the Fe/Mo cations located in the centers of octahedra, whose vertices contain the O(1) and O(2) oxygen anions [8–10].

In the ideal SFMO structure, iron and molybdenum cations have the valence of $Fe^{3+}(3d^5)$ and $Mo^{5+}(4d^1)$ and are in the high-spin state with the electronic configurations $3d^5\{t_{2g}^3\uparrow\uparrow\uparrow e_g^2\uparrow\uparrow, S=5/2\}$ и $4d^1,\{t_{2g}^1\downarrow, S=1/2\}$. In a real structure there are zero-dimensional defects of various types, especially antisites (Fe_{Mo}, Mo_{Fe}) and anion vacancies ($V_O^{\bullet\bullet}$). In the presence of iron $Fe^{3+}(3d^5)$ and molybdenum $Mo^{5+}(4d^1)$ cations, due to redistribution of the electron density, the Fe^{2+}, $3d^6\{t_{2g}^4\uparrow\uparrow\uparrow\downarrow e_g^2\uparrow\uparrow, S=2\}$ and Mo^{6+}, $4d^0\{t_{2g}^0, S=0\}$ cations appear [11-13]. The diamagnetic $Mo^{6+}(4d^0)$ cations do not participate in the exchange interactions, so that according to the Kramers-Anderson model only negative exchange interactions are possible between single-charged iron cations. This circumstance leads to the formation of an antiferromagnetic ordering of the magnetic moments and, as a consequence, to the formation of antiferromagnetic inclusions (clusters) in the ferrimagnetic matrix. In this case, the presence of point antisite defects (Fe_{Mo} and Mo_{Fe}) destroys the superstructural ordering, thus having a significant effect on the magnetic structure of SFMO [8-13]. As a result, depending on the concentration of such defects, a ferrimagnetic, antiferromagnetic or mixed magnetic state can be realized. In this case, the magnetic inhomogeneity has a significant effect on the magnetic and electrical characteristics of SFMO.

Neutron-based research techniques are direct methods of studying the evolution of phases present, as well as of various types of clusters formed during thermal processing in the volume of the material. First of all, this refers to the technique of small-angle neutron scattering (SANS). Since the neutrons are not only scattered by the crystal lattice, but also interact with the magnetic moments of the nuclei, the magnetic inhomogeneities contribute to the SANS. The presence of antiferromagnetic clusters in SFMO with an average radius of 20–30 nm was observed by means of SANS [14]. Besides, according to the AC measurements of the magnetic susceptibility, as well of the temperature dependences of the magnetization measured in the field-cooling (FC) and zero-field

cooling (ZFC) regimes in the temperature range from 300–4.2 K, the presence of antiferromagnetic inclusions in the ferrimagnetic matrix was also established. Of particular interest is the studies of the formation dynamics of antiferromagnetic inclusions, changes in their size, fractal dimension and structural organization, depending on the concentration of Fe_{Mo}, Mo_{Fe} point defects and the degree of superstructural ordering of the Fe/Mo cations. Nevertheless, this information is still not available in the literature. This is due to the fact that classical methods such as X-ray and neutron diffraction, electron microscopy, etc., are not applicable to the solution of the problem.

As a consequence, the aim of this paper is to study the effect of the oxygen non-stoichiometry (δ) and degree of superstructural ordering of Fe/Mo cations (***P***) on the formation dynamics, fractal dimension and structural organization of antiferromagnetic imclusions in SFMO.

2. Experimental

Polycrystalline $Sr_2FeMoO_{6-\delta}$ samples were obtained by solid-phase synthesis from partially reduced $SrFeO_{3-x}$, $SrMoO_4$ precursors. The latter were produced using conventional ceramic technology from high-purity MoO_3, Fe_2O_3 oxides and $SrCO_3$ carbonate. Grinding and mixing of the stoichiometric mixture of the initial reagents was carried out in a vibromill in alcohol for 3 hours. The resulting blends were dried at a temperature of 350 K and compressed into pellets. A preliminary annealing in the course of the $SrFeO_{3-x}$, $SrMoO_4$ precursors synthesis was carried out in air at 970 K and 1070 K for 20 and 40 hours, respectively. A repeated grinding was used to increase the homogeneity of the charge. The final synthesis of the $SrFeO_{2.5}$ compound was carried out at T = 1470 K for 20 hours in an argon flux, and of $SrMoO_4$ at T = 1470 K for 40 hours at $p(O_2) = 0.21 \cdot 10^5$ Pa, followed by quenching at room temperature. Pellets from the initial reagents ($SrFeO_{2.5}$ and $SrMoO_4$) of stoichiometric composition were pressed with a diameter of 10 mm, thickness of 4–5 mm, and then annealed in a 5%H_2/Ar gas flux at 1420 K for 5 hours, followed by quenching at room temperature. To avoid kinetic difficulties in establishing the thermodynamic equilibrium of the solid-gas system under investigation, some of the synthesized samples were crushed to submicron sizes in an agate mortar, followed by a treatment in a vibromill in ethyl alcohol for 1 hour.

The oxygen content of the initial SFMO samples was determined by weighing before and after their complete reduction in a gas mixture flux (30% Ar and 70% H_2) at 1473 K for 20 hours to a simple SrO oxide and Fe and Mo metals. It has been established that the initial samples had a single-phase $Sr_2FeMoO_{5.99}$ composition without superstructural ordering of iron and molybdenum cations (***P*** = 0%). The obtaining of samples with different oxygen contents was carried out by

annealing at 1420 K in a flux of a gas mixture of 5% H_2/Ar for 20 hours (*A*–1, $Sr_2FeMoO_{5.97}$, ***P*** = 76%); 50 hours (*A*–2, $Sr_2FeMoO_{5.94}$, ***P*** = 86%) and 90 hours (*A*–3, $Sr_2FeMoO_{5.94}$, ***P*** = 93%).

The crystal lattice parameters were determined using the ICSD-PDF2 (Release 2000) database and the PowderCell, FullProf software [11], using the Rietveld refinement, based on x-ray diffraction data obtained with CuK_α radiation at the Philips X' Pert MPD diffractometer diffractometer. The degree of superstructural ordering of iron and molybdenum cations was calculated by the formula $P = (2 \cdot SOF - 1) \cdot 100\%$, where SOF is the Seat Occupancy Factor. The diffractograms were taken at room temperature at a rate of 60 deg/h in the angular range of θ = 10–90 deg. The Curie temperature of all samples was determined by the ponderomotive technique during measurements of their magnetization in the temperature range from 77–800 K in an external magnetic field of B = 0.86 T.

Measurements of small-angle scattering of unpolarized and polarized neutrons (transmission mode, planar geometry) were carried out at the SANS-1 facility (Helmholtz-Zentrum Geesthacht, Zentrum für Material- und Küstenforschung GmbH, Geesthacht, Germany). The beam was polarized by specular reflection from magnetized optical mirrors, during which, due to the difference in the neutron scattering cross sections for spin states $\pm\frac{1}{2}\hbar$, a polarization level of $0.9 < P_n < 1$ was achieved. The differential scattering cross section per unit volume (scattering intensity I) was obtained as a function of the scattering vector with the modulus $q = (4\pi/\lambda) \cdot \sin(\theta/2)$, where λ = 8.1 Å is the neutron wavelength (non-monochromaticity ~ 10%), and θ is the deflection angle of scattered neutrons from the initial beam direction, which is determined by the position-sensitive detector (PSD) located behind the sample. The measurement range amounted to q = 0.005–0.25 $Å^{-1}$. In the experiments we used a neutron beam with a polarization of $0.9 < P_n < 1$. The experiments were carried out both with and without an applied magnetic field. The field B = 1.5 T was aligned perpendicular to the neutron beam (parallel to the plane of the detector). In the case of polarized neutrons, two types of scattering were measured, corresponding to different polarizations of the beam: along the field (I^-) and opposite to it (I^+). The initial polarization of the neutrons was reversed by a spin-flipper (efficiency > 95%).

3. Results and discussion

According to x-ray phase analysis, samples *A*–1, *A*–2 and *A*–3 with different oxygen indices δ are single-phase without the presence of reflexes of other compounds (**Figure 1**). The presence of the (101) and (103) reflexes indicates the formation of a superstructural ordering of iron and molybdenum cations in the samples.

Author Accepted Manuscript. This article is published in Phys. Status Solidi B 2019, 256, 1800428,
https://doi.org/10.1002/pssb.201800428

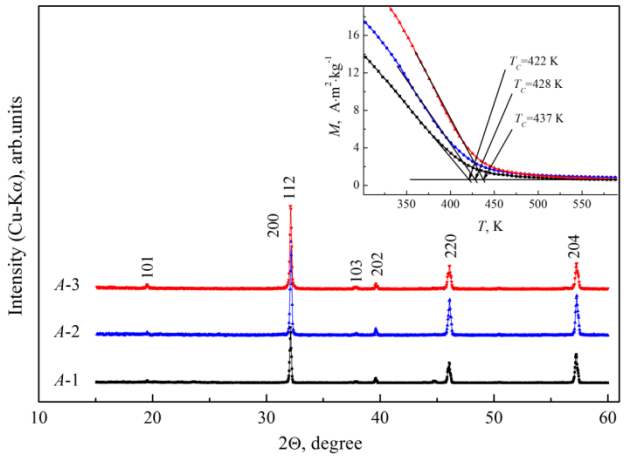

Figure 1 (color online). X-ray diffraction patterns of samples *A*–1, *A*–2 and *A*–3. Insert: temperature dependence of magnetization of the samples, measured in a magnetic field with induction $B = 0.86$ T.

In addition, it was found that as ***P*** increases, the magnetization values $M(T)$ increase in the temperature range from 77–550 K, and at 77 K they are $M(A–1)_{77K} = 26.41$ A m^2 kg^{-1}, $M(A–2)_{77K} = 32.36$ A m^2 kg^{-1} and $M(A–3)_{77K} = 42.66$ A m^2 kg^{-1}. It was found that the samples have different transition temperatures from the paramagnetic to the ferrimagnetic state with the values of $T_C \approx 422$ K, $T_C \approx 428$ K и $T_C \approx 437$ K for $\boldsymbol{P} = 76\%$, $\boldsymbol{P} = 86\%$ и $\boldsymbol{P} = 93\%$, respectively (**Figure 1**).

Based on the study of the temperature dependence of the magnetic moment in the ZFC and FC modes, a magnetically inhomogeneous state was observed in the samples. Thus, in the process of cooling SFMO below T_C at $B = 0$ T, the magnetic moments of the particles m_i are oriented along their easy magnetization axes (EA) in a random manner, with $\vec{M} = \sum_{i=1}^{n} \vec{m}_i = 0$. When placed in an external magnetic field $B \neq 0$, the total energy of the sample volume V, consisting of the energy of the magnetic anisotropy and the interaction energy of the magnetic moment with the external magnetic field B, takes the form:

$$E_M = VMB \cdot \cos\theta + VK \cdot \sin^2\theta, \qquad (1)$$

where V is the grain volume, M is the magnetization, θ is the angle between the magnetization vector and the EA, and K is the uniaxial magnetic anisotropy constant. When a weak external magnetic field with an induction of $B = 0.01$ T is applied, smaller than the coercive force of $\mu_0 H_c = 0.012$, 0.013, 0.014 T for *A–1, A–2* и *A–3*, respectively, followed by an increase in temperature in the range from 4.2 – 22 K a sharp increase in the magnetic moment of the sample is observed (**Figure 2**). This is due to the fact that the magnitude of the potential barrier, obtained as an extremum of the function **Eq. (1)** for a sample placed in an external magnetic field, given by the condition

$$\frac{\partial E}{\partial \theta} = \frac{\partial}{\partial \theta}(KV\sin^2\theta + MBV\cdot\cos\theta) = 0, \qquad (2)$$

exceeds $E_{\text{therm}} = k_B T$, and therefore the process of magnetization reversal of superparamagnetic grains with a volume less than a certain critical value ($V < V_{cr}$) occurs coherently: all their spins rotate so that they remain oriented parallel to each other, while the B field is not sufficient for the magnetization reversal of the non-paramagnetic grains. Therefore, with a further increase in temperature, the magnetization of the samples only decreases [15, 16]. It should be pointed out that other authors [17, 18] also observed superparamagnetic properties of the double perovskite $Sr_2FeMoO_{6-\delta}$ containing quasispherical grains with dimensions $d \sim 40$–100 nm, in the temperature dependences of the magnetic moment.

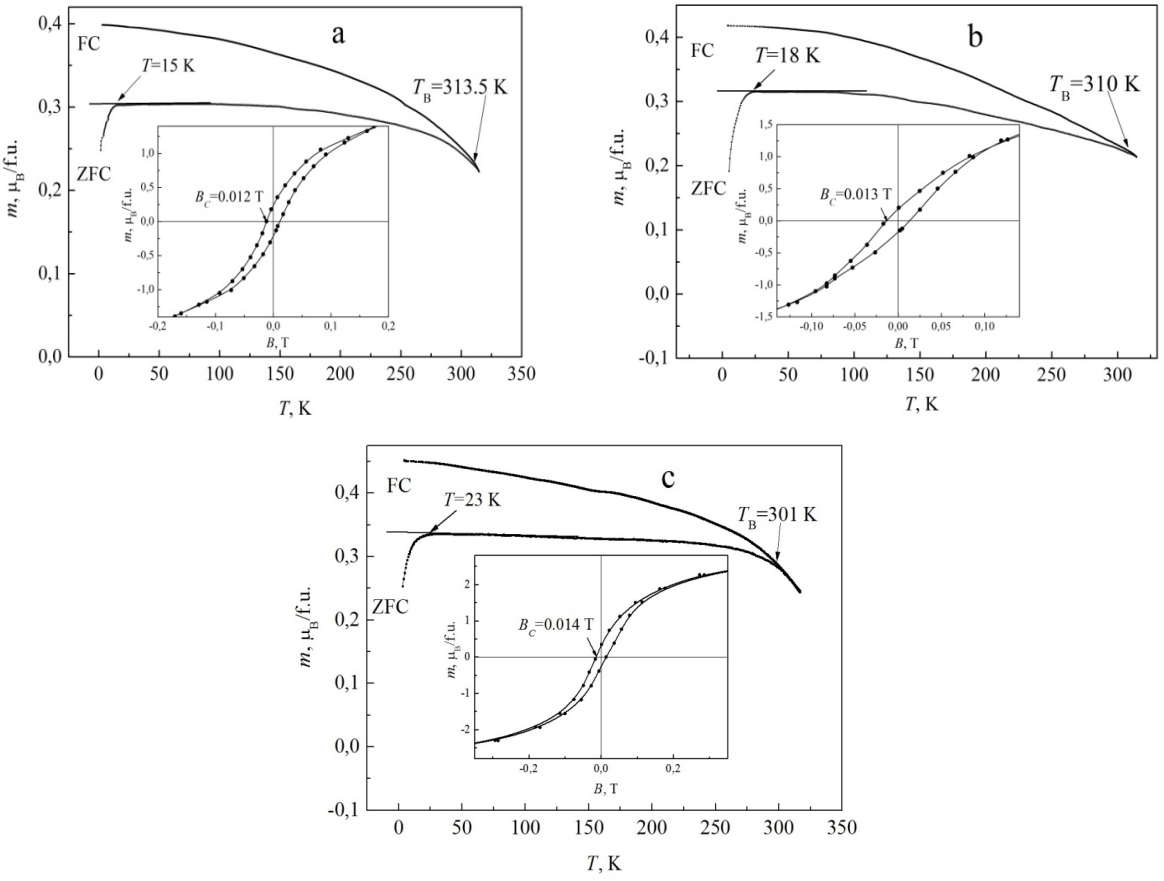

Figure 2. Temperature dependences of the magnetic moment of samples *A*–1 (a), *A*–2 (b), *A*–3 (c), measured in the ZFC and FC regimes. The insets show the field dependences of the magnetic moment of the samples.

With a further increase in temperature, a smooth decrease in m_i is observed, which is due to the contribution of thermal fluctuations with energy $E_{\text{therm}} = k_B T$ to the demagnetization of superparamagnetic grains. The magnetic field induction $B = 0.01$ T is smaller than $\mu_0 H_c$, so that

there is no contribution of non-magnetic grains to the magnetization of samples *A*–1, *A*–2 and *A*–3 up to the blocking temperature T_B. In this case, the increase in the ***P*** values also affects the magnetic moment per formula unit that equals $m(A–1) = 1.33\ \mu_B$/f.u., $m(A–2) = 3.07\ \mu_B$/f.u. and $m(A–3) = 3.58\mu_B$/f.u. at $T = 77$ K, which correlates well with the degree of superstructural ordering of the Fe/Mo cations: ***P***(*A*–1) = 76%, ***P***(*A*–2) = 86%, ***P***(*A*–3) = 93%. Since the magnetic moment in the double perovskite SFMO is determined by the ferrimagnetic ordering of the magnetic moments of cations in the high-spin state, viz., $Fe^{3+}(3d^5, t_{2g}^3\uparrow\uparrow\uparrow e_g^2\uparrow\uparrow, S = 5/2)$ and $Mo^{5+}(4d^1, t_{2g}^1\downarrow, S = 1/2)$, the lower values of $M(A–1)_{77K}$ are due to the transition of some Fe cations to the lower valent state.

The presence of a magnetically inhomogeneous state in samples containing magnetic regions of different magnetic nature is indicated by the SANS data. **Figure 3** shows scattering curves for samples *A*–1, *A*–2 and *A*–3 in the absence and in the presence of an external magnetic field.

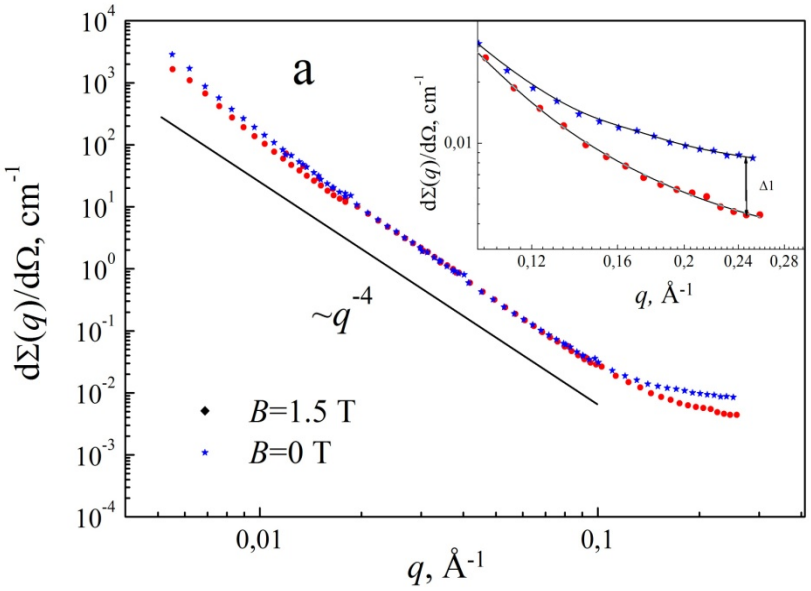

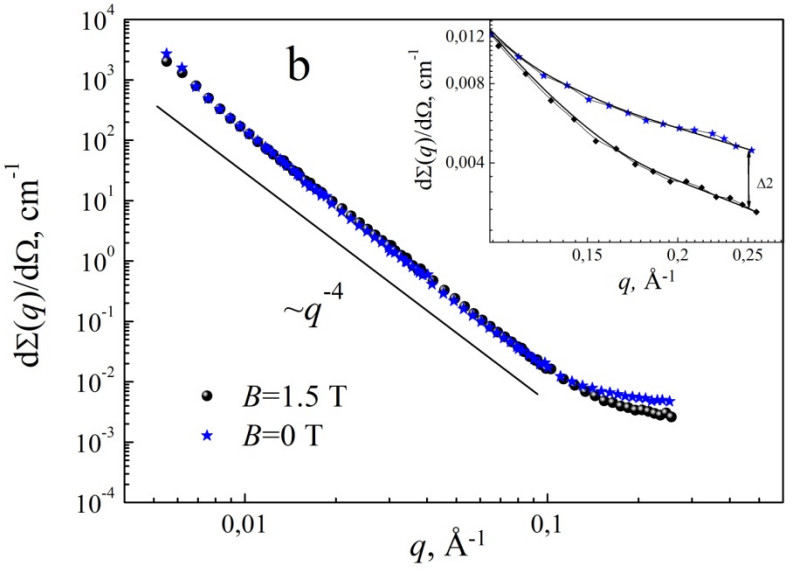

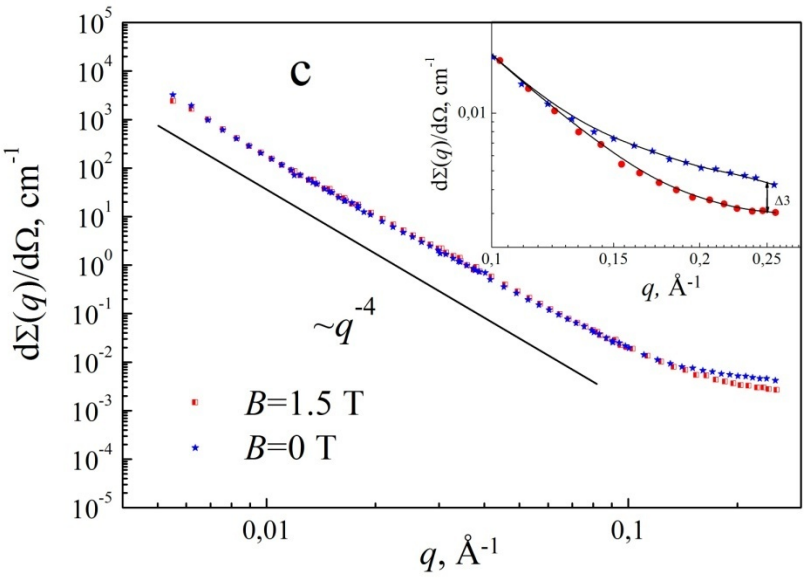

Figure 3 (color online). The intensity of small-angle scattering of unpolarized (B = 0) and polarized (B = 1.5 T) neutrons for samples (a) A–1, (b) A–2 and (c) A–3. For samples in a magnetic field, the intensity $(I^+ + I^-)/2$, averaged over the area of the PSD, is shown. The solid line shows the intensity decay according to the Porod law $I \sim q^{-4}$.

It is known that when polarized neutrons pass through a magnetic medium with an arbitrary orientation of the magnetic domains, neutrons are depolarized due to dephasing as a result of the Larmor precession. This process can also be described as small-angle scattering in a magnetic medium. Thus, the depolarization of neutrons characterizes the magnetic homogeneity of the medium. To avoid or, at least, minimize depolarization, it is necessary to magnetize the samples to saturation [19-21]. The results of our studies indicate that a magnetic field of 1.5 T destroys the original magnetic structure of the double perovskite samples. Therefore, in order to elucidate the effect of magnetic clusters on the scattering of neutrons, we applied an external magnetic field with induction B = 1.5 T. The induction value was chosen to be above the coercivity and close to the saturation, so that the condition $B \sim B_{sat} > \mu_0 H_c$ is satisfied. It has been found that the magnetic field affects the scattering curve only in the region of large scattering vectors ($q > 0.1$ Å^{-1}).

For the characterization of the formed A–1, A–2 and A–3 structures, a power law was used to approximate the SANS behaviour [22]:

$$d\Sigma(q)/d\Omega = Aq^{-\alpha} + B, \qquad (1)$$

where $d\Sigma/d\Omega$ is the differential neutrons scattering cross-section, Ω is the neutrons scattering solid angle, α is the exponent of the power law, $A = 2\pi\Delta\rho^2 S$ is a parameter characterizing the inhomogeneities total surface area, S is the specific interface area between the inhomogeneity and

the matrix, B is the residual incoherent background, $\Delta\rho^2 = (\rho - \rho_s)^2$ is the contrast, where ρ and ρ_s are the average densities of the neutron scattering lengths for the particle and the matrix, correspondingly. The α value indicates the presence of the types of structures which cause scattering in different intervals of the scattering vector q values.

For samples A–1, A–2 and A–3, for all B values and for the wave vectors in the interval $0.1 > q > 0.002$ Å^{-1}, the exponent is on the order of four ($\alpha \cong 4$) (**Figure 3**). This indicates that scattering on magnetic structures with a large characteristic lengths ($D > 6$ nm) obeys the Porod law $I \sim q^{-4}$ [23], which corresponds to an object with a smooth, well-marked surface and polydisperse grain sizes (**Figure 4**).

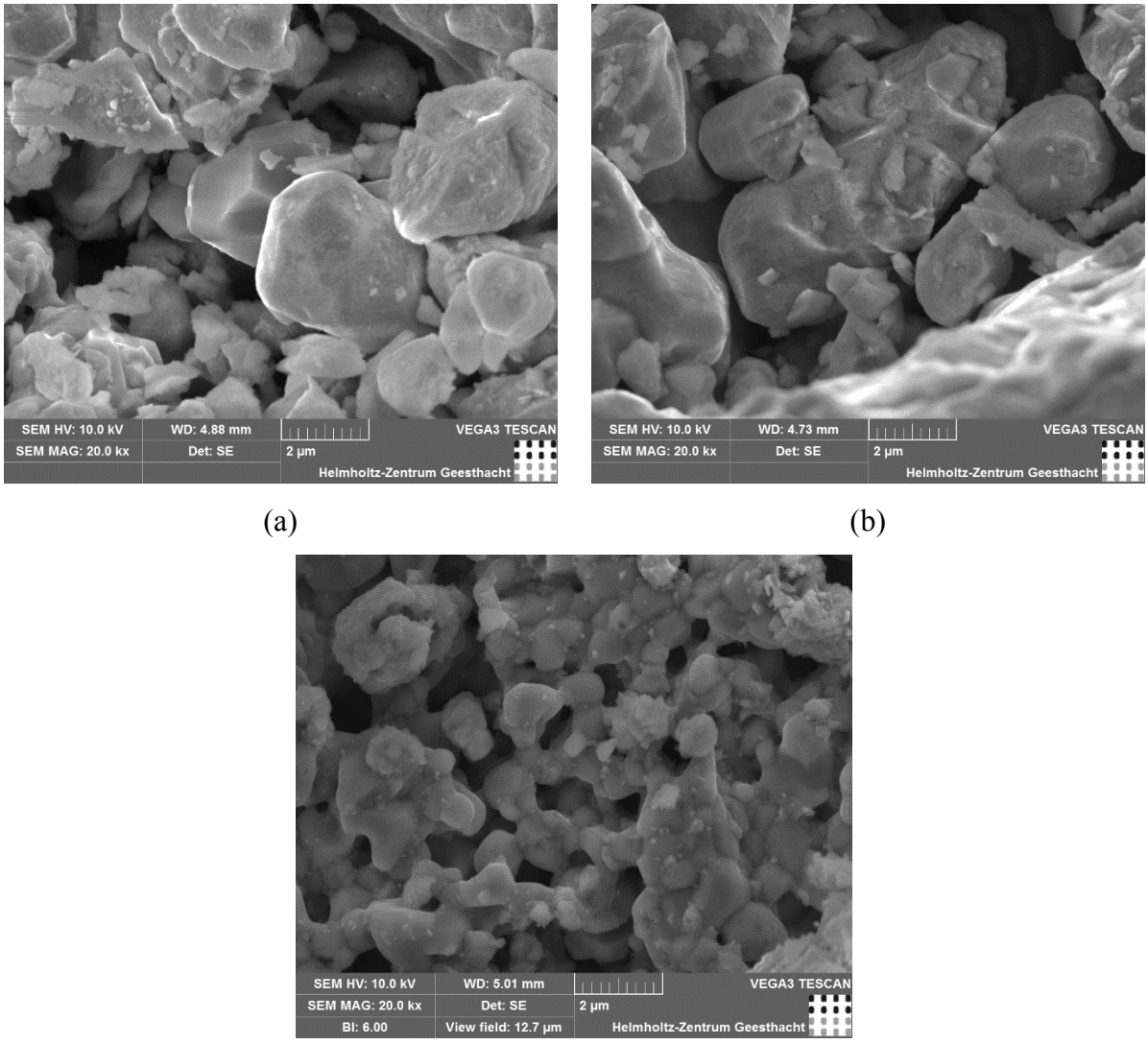

(a) (b)

(c)

Figure 4. Microstructure of the samples (a) A–1, (b) A–2 and (c) A–3, observed in the SEM.

An important result is the observed difference between the slope of the SANS curves of samples A–1, A–2 and A–3, which indicates a different microstructure of the inhomogeneities. The

main inhomogeneities at which scattering occurs are magnetic inclusions with characteristic dimensions that depend on the superstructural ordering of Fe/Mo. For $q > 0.1$ A^{-1}, the scattering curves obtained on *A*–1, *A*–2 и *A*–3 in magnetic fields up to 1.5 T show that the application of a magnetic field leads to a decrease in scattering. This circumstance indicates a certain magnetic contribution from small-scale inhomogeneities (impurities) with $D < 6$ nm which are partially destroyed / oriented by a magnetic field with $B = 1.5$ T. According to the data of small-angle scattering of polarized neutrons, variation dynamics of magnetic inhomogeneities with a size of $D < 6$ nm in samples *A*–1, *A*–2 and *A*–3 are observed. Proceeding from the fact that $\Delta 1 > \Delta 2 > \Delta 3$, where $\Delta = (d\Sigma(q)/d\Omega)_{B=0} - d\Sigma(q)/d\Omega)_{B=1.5T}$ at $q = 0.25$ Å^{-1}, we can conclude that the scattering intensity decreases significantly with increasing ***P***, which witnesses to the reorganization of magnetic structures in the range of small distances.

Thus, it follows from the obtained results that the increase in the magnetization and the Curie temperature with increasing ***P*** can be explained by the presence of antisite defects and oxygen vacancies. The presence of Fe_{Mo}, Mo_{Fe}, and $V_O^{\bullet\bullet}$ stimulates the redistribution of the electron density with a change in the electron configuration of some of the iron and molybdenum ions according to the scheme $Fe^{3+}(3d^5) + Mo^{5+}(4d^1) \rightarrow Mo^{6+}(4d^0) + e + Fe^{3+}(3d^5) \rightarrow Fe^{2+}(3d^6) + Mo^{6+}(4d^0)$. Proceeding from the fact that the diamagnetic cations $Mo^{6+}(4d^0)$ do not participate in the exchange interactions, and only negative exchange interactions are possible between the $Fe^{2+}(3d^6)$ ions having a smaller magnetic moment than the $Fe^{3+}(3d^5)$ ones, the built-up of an antiferromagnetic ordering of the magnetic moments between the $Fe^{2+}(3d^6)$ ions is concluded. A similar situation with a negative exchange integral $J < 0$ was observed in iron-substituted double perovskites (Sr_2BMoO_6, where B = Ni, Co) with $Mo^{6+}(4d^0)$ ions in the molybdenum sublattice [24, 25]. Thus, with an increase in the concentration of the Fe^{2+} ions and of the Fe_{Mo} and Mo_{Fe} antisite defects, the probability of formation of clusters of the type Fe_{Fe}–O–Fe_{Mo} and Mo_{Mo}–O–Mo_{Fe} increases. In this case, a Fe cation located at the Mo site is surrounded by other Fe cations, which leads to the realization of the superexchange interaction according to the Kramers-Anderson mechanism. Moreover, the superexchange interaction should be considered as a direct interaction between the magnetic orbitals of the equally charged – Fe–Fe – and – Mo–Mo – cations through a ligand (oxygen). In this case, the exchange interaction should be regarded as a perturbation, which makes it possible for the transition of the *p*-electron of oxygen to the *d*-orbital of the iron cation without changing the singlet to the triplet state and mixing states of different multiplicity. In such a superexchange interaction, the effective exchange integral is negative and corresponds to the expression [26, 27]

$$-2J = -2\langle\psi_a\psi_b|e^2/r_{1,2}|\psi_b\psi_a\rangle + 2b^2/U, \qquad (2)$$

where b is the electron transfer integral between the orbits belonging to the neighboring cations, e is the electron charge, U is the transfer energy needed to promote the system to the excited state that appears when the electron passes to a neighboring ion, $r_{1,2}$ is the distance between the electrons, ψ_a and ψ_b are the orbital wave functions of the d-electrons of the cations Fe(a, b) or Mo(a, b) located on opposite sides of the ligand.

The presence of antiferromagnetic clusters in the compound reduces the formation probability of long-range ferrimagnetic ordering, which leads to the partitioning of large ferrimagnetic domains into smaller ones due to the system's tendency to minimize the free energy. The latter consists of several components, such as magnetostatic, magnetoelastic, exchange interaction and magnetocrystalline anisotropy energy. In this case, according to the SANS data, the size of the antiferromagnetic inclusions does not exceed $D < 6$ nm, and taking into account $\alpha > -4$, they have a serpentine shape, and their length and concentration increase with increasing concentrations of Fe_{Mo} and Mo_{Fe}.

It is logical to assume that the magnetically inhomogeneous state with ferrimagnetic short-range ordering of spins of the Fe/Mo cations in samples *A*–1, *A*–2 и *A*–3 is due to the frustration of the exchange bonds and the realization of various magnetic states – antiferromagnetic, ferrimagnetic and superparamagnetic, when the spin inversion does not change the energy of the system in a wide range of temperatures.

4. Conclusions

Based on the measurements of the magnetic characteristics, it has been established that an increase in the magnetization (26.41 A m^2 kg^{-1}, 32.36 A m^2 kg^{-1} and 42.66 A m^2 kg^{-1}), magnetic moment (1.33 μ_B/f.u., 3.07 μ_B/f.u. and 3.58 μ_B/f.u. at $T = 77$ K) and Curie temperature (422 K, 428 K and 437 K) in SFMO with increasing ***P*** (76%, 86% and 93%) can be explained by the presence of antisite defects and antiferromagnetic inclusions. The temperature dependences of the magnetic moment measured in the ZFC and FC regimes have indicated a magnetically inhomogeneous state in the samples. The same conclusion has been drawn also from the SANS data. For samples *A*–1, *A*–2 and *A*–3 for all values and directions of the field B, the α value was approximately equal to 4 for the wave vectors in the interval $0.1 > q > 0.002$ $Å^{-1}$. This means that scattering by magnetic inhomogeneities with large characteristics lengths ($D > 6$ nm) obeys the Porod law, which corresponds to an object with a smooth and well-marked surface and polydisperse grain sizes. Deviations from the Porod law for $q > 0.1$ $Å^{-1}$ can be ascribed to magnetic inhomogeneities smaller than 6 nm which are partially destroyed / oriented by magnetic fields $B \geq$

1.5 T. It has been found that the magnetic homogeneity of $Sr_2FeMoO_{6-\delta}$ is improved with increasing superstructural ordering of the Fe/Mo cations.

Acknowledgements

The support of the work in frames of the European project H2020 – MSCA – RISE – 2017 – 778308 – SPINMULTIFILM, the Deutsche Forschungsgemeinschaft (DFG) Project No. SE 2714/2-1, and the Portuguese project I3N/FSCOSD (Ref. FCT UID/CTM/50025/2013) is gratefully acknowledged.

References

[1] J. Cibert, J.-F. Bobo, U. Lüders. C. R. Physique **2005**, *6*, 977.

[2] N. Kalanda, D.-H. Kim, S. Demyanov, S.-C. Yu, M. Yarmolich, A. Petrov, S.K. Oh. Curr. Appl. Phys. **2018**, *18 (1)*, 27.

[3] L.V. Kovalev, M.V. Yarmolich, M.L. Petrova, J. Ustarroz, H. Terryn, N.A. Kalanda, M.L. Zheludkevich. ACS Appl. Mater. Interfaces **2014**, *6 (21)*, 19201.

[4] D. Serrate, J.M. De Teresa, M.R. Ibarra. J. Phys.: Condens. Matter. **2007**, *19*, 023201.

[5] N. Kalanda, S. Demyanov, W. Masselink, A. Mogilatenko, M. Chashnikova, N. Sobolev, O. Fedosenko. Cryst. Res. Technol. **2011**, *46(5)*, 463.

[6] N.A. Kalanda, S.E. Demyanov, A.V. Petrov, D.V. Karpinsky, M.V. Yarmolich, S.K. Oh, S.C. Yu, D.-H. Kim. J. Electron. Mater. **2016**, *45 (7)*, 3466.

[7] K.-I. Kobayashi, T. Kimura, H. Sawada, K. Terakura, Y. Tokura. Nature **1998,** *395*, 677.

[8] R. Allub, O. Navarro, M. Avignon, B. Alascio. Physica B: Condens. Matter. **2002**, *320(1)*, 13.

[9] J. Rager, M. Zipperle, A. Sharma, L. MacManus-Driscoll. J. Am. Ceram. Soc. **2004**, *87*, 1330.

[10] J.P. Zhou, R. Dass, H.Q. Yin, J.-S. Zhou, L. Rabenberg, J.B. Goodenough. J. Appl. Phys. **2000**, *87***,** 5037

[11] Z. Szotek, W. M. Temmerman, A. Svane, L. Petit, H. Winter. Phys. Rev. B. **2003**, *68*, 104411.

[12] B. Martinez, J. Navarro, L.I. Balcells, J. Fontcuberta. Phys.: Condens. Matter. **2000**, *12*, 10515.

[13] D.D. Sarma, P. Mahadevan, T. Saha-Dasgupta, S. Ray, A. Kumar, Phys. Rev. Lett. **2000**, *85*, 2549.

[14] V. Kanchana, G. Vaitheeswaran, M. Alouani, A. Delin. Phys. Rev. B. **2007**, *75*, 2204041.

[15] N.A. Kalanda, L.V. Kovalev, J.C. Waerenborgh, M.R. Soares, M.L. Zheludkevich, M.V. Yarmolich, N.A. Sobolev. Sci. Adv. Mater. **2015**, *7*, 446.

[16] M. Yarmolich, N. Kalanda, S. Demyanov, Ju. Fedotova, V. Bayev, N.A. Sobolev. Phys. Status Solidi B. **2016**, *253 (11)*, 2160.

[17] X.H. Li, Y.P. Sun, W.J. Lu, R. Ang, S.B. Zhang, X.B. Zhu, W.H. Song, J.M. Dai. Solid State Commun. **2008**, *145*, 98.

[18] T. Suominen, J. Raittila, T. Salminen, K. Schlesier, J. Lindén, P. Paturi. J. Magn. Magn. Mater. **2007**, *309 (2)*, 278.

[19] A. Heinemann, A. Wiedenmann. J. Appl. Cryst. **2003**, *36*, 845.

[20] S. Mercone, V.Hardy, C. Martin, C. Simon. Phys. Rev. B **2003**, *68*, 094422.

[21] V. Runov, H. Glattli, G. Kopitsa, A. Okorokov, M. Runova. Physica B **2000**, *276-278*, 795.

[22] D. Saurel, A. Brûlet, A. Heinemann, C. Martin, S. Mercone, C. Simon. Phys. Rev. B **2006**, *73*, 094438.

[23] G. Porod. Small Angle X-ray Scattering (Academic Press, London, 1983), p. 35.

[24] Y. Sui, X.J. Wang, Z.N. Qian, Z.G. Liu, J.P. Miao, J.G. Cheng, X.Q. Huang, Z. Lu, W.H. Su, C.K. Ong. J. Magn. Magn. Mater. **2005**, *290–291 (2)*, 1089.

[25] J.-S. Kang, J.H. Kim, A. Sekiyama, S. Kasai, S. Suga, S.W. Han, K.H. Kim, T. Muro, Y. Saitoh, C. Hwang, C.G. Olson, B.J. Park, B.W. Lee, J.H. Shim, J.H. Park, B.I. Min. Phys. Rev. B. **2002**, *66*, 1131051.

[26] M. Tovar, M.T. Causa, A. Butera, J. Navarro, B. Martinez, J. Fontcuberta, M.C.G. Passeggi. Phys. Rev. B. **2002**, *66*, 024409.

[27] N. Menéndez, M. García-Hernández, D. Sánchez, J.D. Tornero, J.L. Martínez, J.A. Alonso. Chem. Mater. **2004**, *16 (18),* 3565.